

# A Systemic Approach for Pellet Reactor Modeling: Application to Water Treatment

L. Montastruc, C. Azzaro-Pantel, L. Pibouleau, and S. Domenech

Laboratoire de Génie Chimique, UMR 5503 CNRS/INP/UPS, ENSIACET, 31077 Toulouse Cedex 4, France

DOI 10.1002/aic.10254

Published online in Wiley InterScience (www.interscience.wiley.com).

*The development is reported of a model for a fluidized-bed process for phosphate precipitation and removal from wastewater. The general framework of this study involves a two-step procedure. The first modeling level was previously presented elsewhere and leads to the development of a thermodynamic model for the computation of phosphate conversion for the  $\text{Ca-PO}_4\text{-H}_2\text{O}$  system. The second step of the modeling procedure is the core of this report and computes the reactor efficiency from the identification of the so-called pellet reactor model as a reactor network involving a combination of elementary systems representing basic ideal flow patterns (perfect mixed flow, plug flow, and so on). For solving the involved mixed-integer quadratic programming (MIQP) problem, a hybrid procedure based on simulated annealing (SA) and quadratic programming (QP) is implemented. The SA generates reactor network structures deduced from a superstructure and for each one, a QP is carried out. The goal is to find not only the most appropriate model, but also the simplest one (in terms of the smallest possible number of elementary units). Thus the objective function is augmented with an outer penalty quadratic function representing the number of elementary units. The methodology was first validated on an example previously treated with a classical MINLP method involving a limited number of variables. The main interest of the approach proposed here is that it can handle large-size problems with a limited exploration of the search space and can be consequently extended to combinatorial problems. A comparison with experimental results obtained in the pilot unit designed for this study shows the efficiency of the systemic approach.*

© 2004 American Institute of Chemical Engineers AIChE J, 50: 2514–2525, 2004

**Keywords:** model identification, pellet reactor, phosphate, quadratic programming, reactor network, simulated annealing

## Introduction

Phosphorus recovery from wastewater corresponds with the increasing demand of sustainable development of the phosphate industry and the associated stringent environmental quality standards. In this context, numerous engineering solutions, aiming at addressing phosphorus recovery from wastewater by precipitation of calcium phosphates in a recyclable form (Morse et al., 1998), have been proposed in the last decade. An

advanced alternative is to implement the so-called pellet reactor approach (Hirasawa and Toya, 1990, Seckler et al., 1996). The objective of this report is thus to address a real environmental issue by appropriately designing an optimal pellet reactor.

In this framework, a two-step procedure is proposed with  $\text{Ca-PO}_4\text{-H}_2\text{O}$  as a support system (see Figure 1). This article reports on the study of the precipitation features of calcium phosphate in a fluidized bed reactor in a concentration range between 50 and 4 mg/L. The first modeling level was previously presented in detail (Montastruc et al., 2003) and leads to the development of a thermodynamic model for predicting phosphate conversion for the  $\text{Ca-PO}_4\text{-H}_2\text{O}$  system. It is im-

Correspondence concerning this article should be addressed to L. Pibouleau at Luc.Pibouleau@ensiacet.fr.

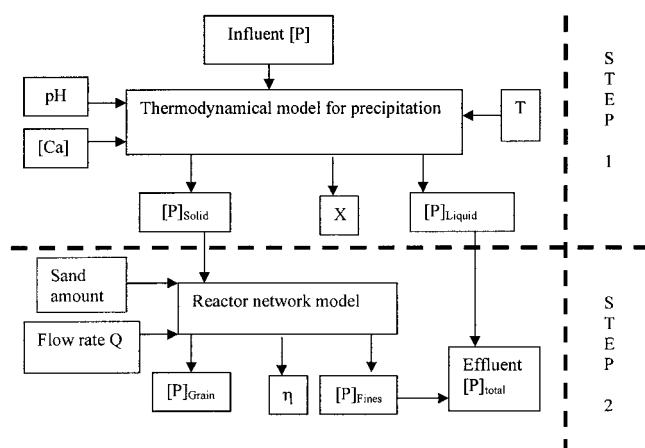


**Figure 1. Principles of pellet reactor modeling.**

portant to recall, however, that the computation of the evolution of phosphate conversion rate as a function of pH, with respect to precipitation of the different calcium phosphate species, implies mass and electroneutrality conservation balances as well as supersaturation relations.

The second step of the modeling procedure is the core of this report and involves the computation of the pellet reactor efficiency. It must be emphasized that a phenomenological way to treat the problem would imply the precise knowledge of some key parameters of the induced agglomeration process (such as coating), which are in fact difficult to obtain practically, such as calcium phosphate density and thickness.

For this purpose, another alternative is proposed herein based on a reactor network-oriented model: the pellet reactor model is actually identified as a combination of elementary systems, representing basic ideal flow patterns (perfect mixed flows, plug flows, and so on). The arrangement of elementary units finally selected must represent—as adequately as possible—the pellet reactor in terms of number of elementary units, volume, and flow rate for each elementary cell, given the total flow rate, the inlet concentration, the total reactor volume, and the outlet concentration. A superstructure, involving the set of all possible solutions corresponding to the physical reactor, has to be defined. Then, potential solutions are extracted from the superstructure and evaluated according to a given objective function.

This article is organized as follows. The first section describes the typical features of the process used for calcium phosphate precipitation and the equipment unit used throughout the study. The performance process indicators, based on the conversion of phosphate from liquid to solid phase and on phosphate removal efficiency, are also presented. The second section clarifies the underlying assumptions of the mathematical formulation for pellet reactor modeling. This constitutes a master problem (structure optimization) using a stochastic procedure and a slave problem (continuous variables optimization, that is, flow rates and volumes) based on a classical quadratic programming technique. The use of a superstructure at the master level is then justified and constitutes a key point of the proposed strategy. The identification procedure for agglomeration rate is also explained. In the third section, the superstructure approach is tested for validation purpose on a previously

treated example (Floquet et al., 1989) related to a settling tank model. The fourth section illustrates the solution strategy for fluidized bed modeling with superstructure embedding. The model parameters are determined by comparison with the experimental data. The objective function to be minimized is the quadratic deviation between experimental and modeled agglomeration rates, augmented with an outer quadratic function representing the number of elementary units. The goal is to find simultaneously the most appropriate model with respect to the experimental output, but also the simplest model, that is, the model involving the smallest possible number of elementary units, that constitutes a key point for future control purposes of the process. The implementation of the simulated annealing procedure used as master problem optimization and the choice of its main parameters (number of cooling stages for the stopping criterion, reducing factor of the temperature, length of cooling stage) are discussed in the fifth section.

Finally, the main results obtained are summarized and some perspectives of this work are given.

## Process Description

The process is based on calcium phosphate precipitation obtained by mixing a phosphate solution with calcium ions and a base. More precisely, it involves a fluidized bed of sand continuously fed with aqueous solutions (see Figure 2). Calcium phosphate precipitates upon the surface of sand grains; at the same time, small particles, also called “fines,” leave the bed with the remaining phosphate not recovered in the reactor. Two different regimes were experimentally observed (see Figure 3). On the one hand, for high values of fluidization velocity ( $>90$  L/h), only one zone is observed at the bed top, in which fines leave the bed with the liquid effluent. Process efficiency is thus mainly attributed to fine coating on sand grains. On the other hand, for low values of fluidization velocity ( $<50$  L/h), an additional layer is observed at the upper zone of the fluidized bed where fines stagnate and agglomerate. Because of the stratified form and size of the agglomerates, the fines remain at

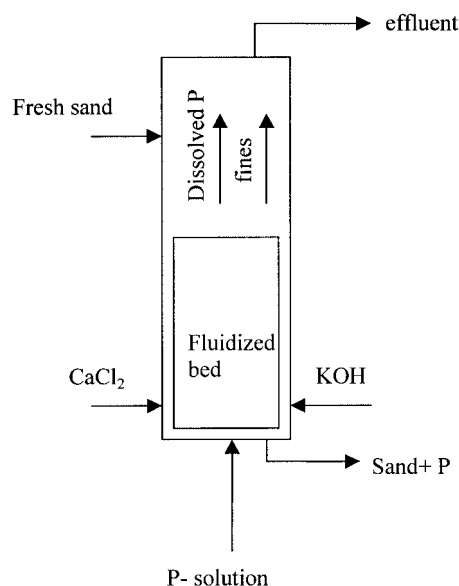


**Figure 2. Pellet reactor.**

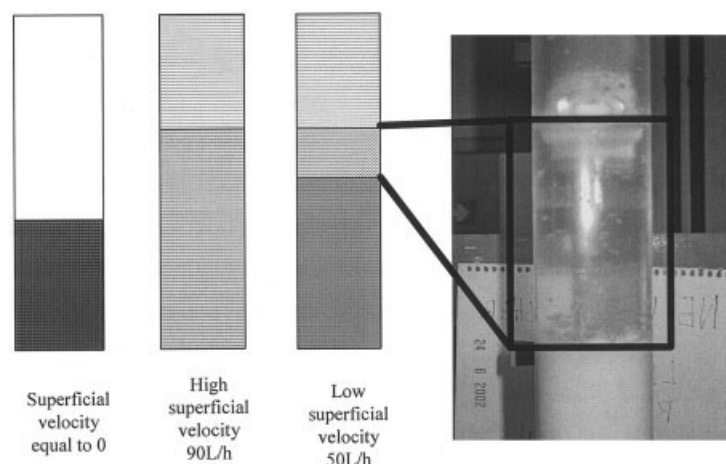
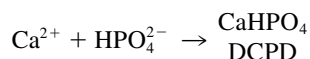
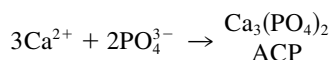


Figure 3. Physical phenomena occurring into the column.

the surface of the bed. Inside the fluidized bed, fines totally cover the sand grains and constitute large particles of complex structure.

It has been suggested elsewhere (Montastruc et al., 2003) that the modeling of fines production involves amorphous calcium phosphate (ACP) for the higher pH values, and both ACP and DCPD (dicalcium phosphate dihydrate) for lower pH values according to the following reaction schemes



Both total and dissolved concentrations of phosphorus, pH, and temperature were measured at the outlet stream. To measure the dissolved concentrations, the upper outlet stream was filtered over a 0.45- $\mu\text{m}$  filter. The sample of total phosphorus was pretreated with HCl to dissolve any suspended solids. The phosphate removal efficiency ( $\eta$ ) of the reactor and the conversion of phosphate from liquid to solid phase ( $X$ ) are defined as

$$\eta = \frac{w_{p,\text{in}} - w_{p,\text{tot}}}{w_{p,\text{in}}} \quad (1)$$

$$X = \frac{w_{p,\text{in}} - w_{p,\text{sol}}}{w_{p,\text{in}}} \quad (2)$$

where  $w_{p,\text{in}}$  represents the flow rate of the phosphorus component at the reactor inlet,  $w_{p,\text{tot}}$  gives the total flow rate of phosphorus both dissolved and in fines at the reactor outlet, and  $w_{p,\text{sol}}$  is the flow rate of dissolved P at the reactor top outlet. If  $\eta_{\text{agg}}$  is the agglomeration rate, which is the ratio between phosphorus in the bed and in the inlet stream, the following relation can be deduced

$$\eta = \eta_{\text{agg}} X \quad (3)$$

The precipitation phenomenon is considered as an agglomeration process, and is represented by Smoluchowski's equation (Mullin, 1993), expressed as

$$\frac{dN_i}{dt} = -kN_iN_j \quad (i = \text{fines}, j = \text{grains}) \quad (4)$$

that is

$$\frac{dC_i}{dt} = -KC_iN_j \quad (5)$$

where  $N$  is the particle concentration ( $\text{m}^{-3}$ ),  $C$  is the concentration ( $\text{mg}/\text{m}^3$ ), and  $K$  and  $k$  represent kinetic constants ( $\text{m}^3 \text{s}^{-1}$ )

$$N_j = \frac{1 - \varepsilon}{\frac{4}{3} \pi r_j^3} \quad (6)$$

The bed porosity  $\varepsilon$  is calculated from a modified Kozeny-Carman equation, as follows

$$\frac{\varepsilon^3}{1 - \varepsilon} = 130 \left[ \frac{\nu_{\text{sup}}^{1.2} v^{0.8}}{g(2r_j)^{1.8}} \right] \left( \frac{\rho_l}{\rho_s - \rho_l} \right) \quad (7)$$

where  $r_j$  is the grain radius,  $\nu_{\text{sup}}$  is the superficial velocity ( $\text{m}/\text{s}$ ),  $\nu$  is the kinematic viscosity ( $\text{m}^2/\text{s}$ ), and  $\rho$  is the density ( $\text{kg}/\text{m}^3$ ).

The height of the bed is then given by (where  $D$  is the column diameter)

$$L = \frac{M}{\frac{\pi}{4} D^2 (1 - \varepsilon) \rho_s} \quad (8)$$

The grains covered with phosphate are removed from the bottom of the bed and replaced intermittently by fresh sand

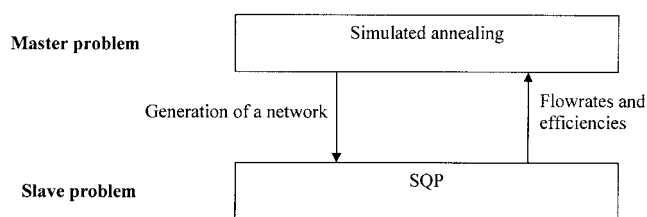


**Figure 4. Two-step solution procedure.**

grains. From many studies reported in the literature (Morse et al., 1998), the phosphate removal efficiency of a single-pass reactor, even at industrial scale, has an order of magnitude of only 50%. It has been shown (Montastruc et al., 2002) that the pellet reactor efficiency depends not only on pH, but also on the hydrodynamic conditions.

## Modeling Principles

Two models are successively used to compute the reactor efficiency. At the first level (see Figure 1), the thermochemical model determines the quantity of phosphate both in the liquid and solid phase vs. pH value, temperature, and calcium concentration. Moreover, this model quantifies the produced amount of ACP and DCPD as a function of the initial conditions (Montastruc et al., 2003).

In classical approaches, the second step involves an agglomeration model requiring as data (Mullin, 1993) the density value of the calcium phosphates that have precipitated in the pellet reactor and also diameter of the fines. Furthermore, the agglomeration rate depends on the hydrodynamic conditions, particularly the eddy sizes. The experimental determination of these values is not straightforward and their estimation requires a lot of assumptions that are difficult to verify practically. For these reasons, this solution was not adopted in the second step.

An alternative is to compute the pellet reactor efficiency, from the identification of the pellet reactor model as a reactor network involving a combination of elementary systems, representing basic ideal flow patterns (perfect mixed flows, plug flows, and so on).

Each elementary system is characterized by specific parameters such as volume and flow rate. The goal is to determine the reactor network representing as adequately as possible the pellet reactor, that is, the number of elementary units and the volume and flow rate for each elementary unit, given the total flow rate, the inlet concentration, the total reactor volume, and the outlet concentration.

## Solution without superstructure

For reactor network identification, several studies use stochastic methods (that is, genetic algorithms or simulated annealing) without embedding the set of possible solutions within a superstructure (Athier et al., 1997; Laquerbe et al., 2001). In that case, the solving strategy is based on a master problem (that is, a stochastic method) that proposes network structures to the slave problem for the optimization of the continuous variables (such as flow rates and volumes) corresponding to each cell arrangement (such as by a QP or SQP method). Yet, this strategy requires a test procedure for detecting the infeasibility of some structures proposed by the stochastic method.

**Table 1. Comparison Between Experimental and Computed Reactor Efficiency for an Input Flow Rate of 90 L/h**

pH	Experimental Conversion Rate	Experimental Efficiency	Computed Efficiency
7.17	0.320	0.220	0.168
7.2	0.344	0.210	0.180
7.5	0.588	0.313	0.308
7.53	0.612	0.299	0.320
7.8	0.783	0.388	0.409

This detection, based on physical concepts, is strongly linked to the problem under consideration and suffers from a lack of generalization. Consequently, an alternative approach involving a superstructure was used in this study.

## Solution within a superstructure

Another strategy consists in using a stochastic procedure for extracting potential solutions from a superstructure. The main advantage is that the problem size (in terms of numbers of both variables and constraints) remains constant and all the solutions proposed by the stochastic method thus become feasible. However, a superstructure that involves the set of all possible solutions corresponding to the physical reactor is required. This approach is not universal, however, because the quality of the obtained solution depends on the superstructure formulation. If some particular solutions cannot be generated from the superstructure, they cannot compete in the optimization procedure. This point may be crucial for complex problems involving an important number of elementary models. Given that the process to be modeled here (that is, a fluidized bed with recycle streams at different levels of the bed) is structurally quite simple, the superstructure approach was finally retained.

## Resolution procedure

The goal is to determine the best reactor network, but also the value of kinetic constant of the associated agglomeration rate, which depends on the reactor network. As previously mentioned, the resolution method is a two-step procedure (as illustrated in Figure 4), where, at the highest level, a simulated annealing procedure extracts a reactor configuration from the superstructure and its corresponding operating conditions are optimized at the lowest level by an SQP method.

## Identification procedure for agglomeration rate

Because the proposed kinetic law is of the first order (see Eq. 4), the concentration influence is null. Thus for each value of both flow rate and pH, the agglomeration rate is obtained by

**Table 2. Comparison Between Experimental and Computed Reactor Efficiency for an Input Flow Rate of 50 L/h**

pH	Experimental Conversion Rate	Experimental Efficiency	Computed Efficiency
7.23	0.371	0.273	0.275
7.26	0.389	0.280	0.288
7.57	0.641	0.448	0.468
7.78	0.773	0.599	0.573
8.02	0.859	0.710	0.637

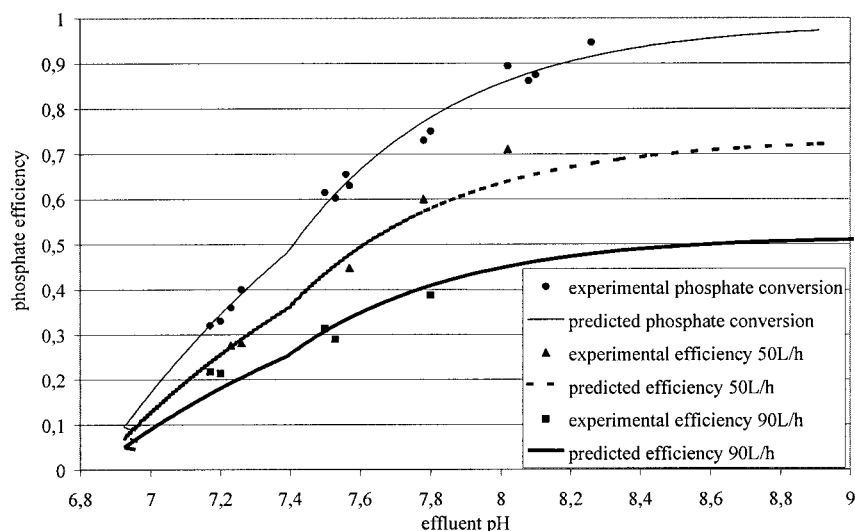


Figure 5. Comparison between experiment and modeling.

minimizing the quadratic deviation between the computed and experimental rates. The reactor efficiency, deduced from the agglomeration rate, is equal to 0.523 for an input flow rate of 90 L/h and 0.742 for an input flow rate of 50 L/h. In Tables 1 and 2 and Figure 5, the efficiency computed from the agglomeration rate is compared with the experimental values for both flow rates. The predicted model curve fits the experimental points quite well; the kinetic law can thus be considered as a first-order reaction. Furthermore, to reduce the complexity of the objective function, for the reactor network, the output concentration computation is based on the agglomeration rate  $(1 - \eta_{agg})$  (see the following section).

### Superstructure Approach Validation

The considered example is adapted from the model identification of a wastewater treatment tank. This example was already treated (Floquet et al., 1989) with a deterministic MINLP procedure, based on the generalized Benders's decomposition. The settling tank is a rectangular tank with two agitators; the superstructure is shown in Figure 6, where DZ refers to a dead zone. The reactions occurring in the tank are of type  $A \rightarrow R$  with a first-order reaction rate  $r_A = KC_A$ .

The goal is to obtain simultaneously the most appropriate model with respect to a given experimental output concentration, but also the simplest model, that is, the model involving the smallest possible number of elementary units. Thus, an

outer penalty quadratic function, representing the number of elementary units, is added to the initial objective function representing the quadratic deviation between the modeled  $C_{fmod}$  and experimental output  $C_{fexp}$ ; so the objective function becomes

$$F = (C_{fmod} - C_{fexp})^2 + \rho \sum_i y(i)^2 \quad (9)$$

where  $\rho$  is a penalty coefficient and  $y$  is the vector of binary variables  $y(i)$  representing the presence or absence of units in the superstructure.

The problem data are the following:

- $F_0 = 36 \text{ m}^3/\text{h}$
- $C_0 = 1 \text{ mol/m}^3$  (inlet concentration)
- $C_f = 0.18 \text{ mol/m}^3$  (outlet concentration)
- $V_0 = 300 \text{ m}^3$  (total volume of the tank)
- $K = 0.36 \text{ h}^{-1}$

The problem involves 13 continuous variables, nine binary variables, and only one linear constraint. The penalty coefficient value has been adjusted, so that both terms  $(C_{fmod} - C_{fexp})^2$  and  $\rho \sum_i y(i)^2$  have the same order of magnitude. A value of  $10^{-3}$  was chosen for the penalty coefficient.

Because the problem combinatorics have been reduced ( $2^9 = 512$  possible structures), all the solutions have been enumerated exhaustively and the best solution is reported in Figure 7. If the output concentration  $C_{fexp}$  is increased to 0.58, the new best solution is given in Figure 8, where it can be observed that the reaction volume is strongly reduced. Note that Figures 7

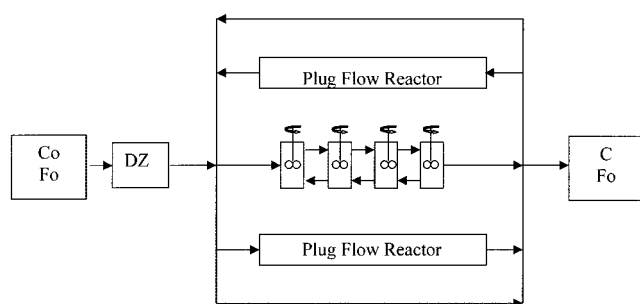


Figure 6. Problem superstructure for the settling tank.

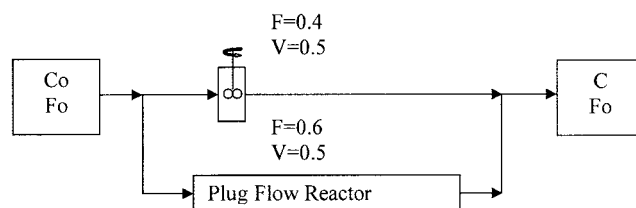


Figure 7. Best solution for  $C_f = 0.18$ .

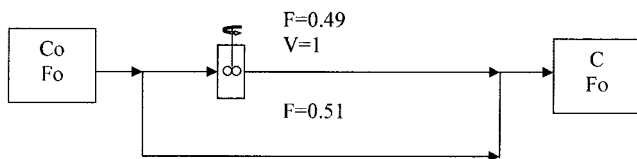


Figure 8. Best solution for  $C_f = 0.58$ .

and 8 refer to reduced volumes. Of course, it must be emphasized that the same results as those obtained in the previous study (Floquet et al., 1989) were found. Yet, the classical MINLP procedure rapidly showed its limit for the treatment of large-size problems, which is typically the case in the problem involved in this study.

## Fluidized-Bed Modeling

### Proposed superstructure

A preliminary study showed that the superstructure proposed for the settling tank problem was inadequate to represent the pellet reactor model with a sufficient degree of precision. This explains why a variant of this superstructure was proposed: each plug flow reactor of the previous superstructure was replaced by a series of four well-stirred tank reactors and additional flows were added, as shown in Figure 9. The final superstructure now involves 15 elements, thus leading to a higher combinatorial problem ( $2^{15} = 32,768$  possible solutions). The first volume  $V_1$  corresponds to a dead zone.

The problem formulation implies the following equations (where  $V_i$ ,  $F_i$ , and  $C_i$  represent, respectively, the reactor volumes, the total flow rates, and the molar concentrations in fines), whereas the term  $y(i)$  is related to the presence or absence of element  $i$ .

### Volume Constraint

$$\sum_{i=1}^{13} V_i = V_{total} \quad (10)$$

### Input Node Constraints

$$F_0 + F_{10} + F_{12} + F_{13} = F_1 + F_{11} + F_{14} \quad (11a)$$

$$C_0 F_0 + C_9 F_{10} + C_{17} F_{12} + C_f F_{13} = (F_1 + F_{11} + F_{14}) C_1 \quad (11b)$$

### Output Node Constraints

$$F_5 + F_{11} + F_{14} = F_6 + F_{12} + F_{13} + F_0 \quad (12a)$$

$$C_5 F_5 + C_{13} F_{11} + C_1 F_{14} = C_f (F_6 + F_{12} + F_{13} + F_0) \quad (12b)$$

**Balances on Reactors.** These equations have the following form (example for reactor 7)

$$C_1 F_1 + C_8 F_9 = C_2 F_2 + C_9 F_{10} + k V_6 C_2 \quad (13a)$$

$$\begin{aligned} F_1 + y(7) F_9 &= F_2 + y(7) F_{10} \\ [1 - y(7)] F_9 &= [1 - y(7)] F_{10} \end{aligned} \quad (13b)$$

That is, four total balance equations and 12 partial balance equations, given that total balance equations for reactors without recirculation streams cannot be written.

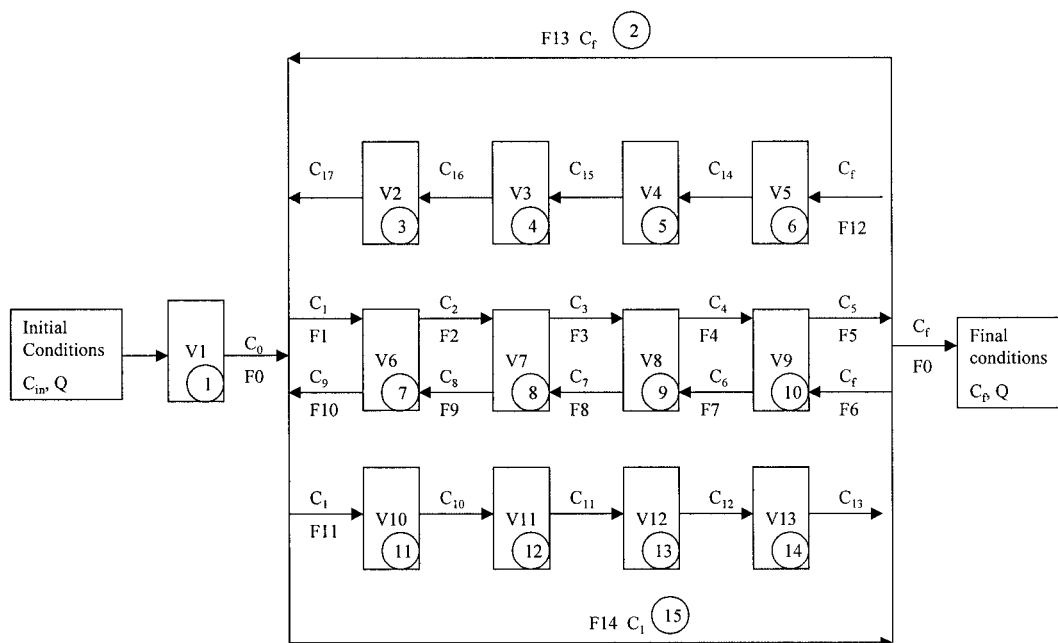


Figure 9. Superstructure for the fluidized bed reactor.

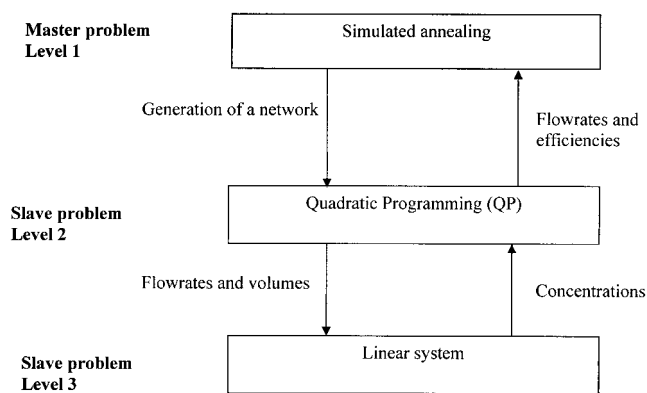


Figure 10. Solution strategy.

### Concentration Equations

$$C_9 = y(7)C_2 + [1 - y(7)]C_8 \quad (14a)$$

$$C_8 = y(8)C_3 + [1 - y(8)]C_7 \quad (14b)$$

$$C_7 = y(9)C_4 + [1 - y(9)]C_6 \quad (14c)$$

$$C_6 = y(10)C_5 + [1 - y(7)]C_f \quad (14d)$$

### Bounds on Variables

$$0 \leq V_i \leq 1 \quad (15a)$$

$$0 \leq C_i \leq 1 \quad (15b)$$

$$0 \leq F_i \leq 1 \quad \text{except for } i = 1 \text{ to } 5, 0 \leq F_i \leq 4 \quad (15c)$$

The optimization problem involves the following items.

#### Linear Constraints

- 1 equation for the volumes
- 8 total balance equations on the reactors
- 2 total balance equations on nodes
- 4 concentration equations

#### Bilinear Constraints

- 2 partial balance equations on nodes
- 12 partial balance equations on the reactors

#### Bounded Variables

- 13 volumes
- 14 flow rates

The objective function to be optimized (by using a QP procedure from IMSL library) for each proposed structure can be written as follows

$$\min(F) = \lambda(C_{f \text{ mod}} - C_{f \text{ exp}})^2 + (1 - \lambda)(C_{f \text{ mod}} - C_{f \text{ exp}})^2 \quad (16)$$

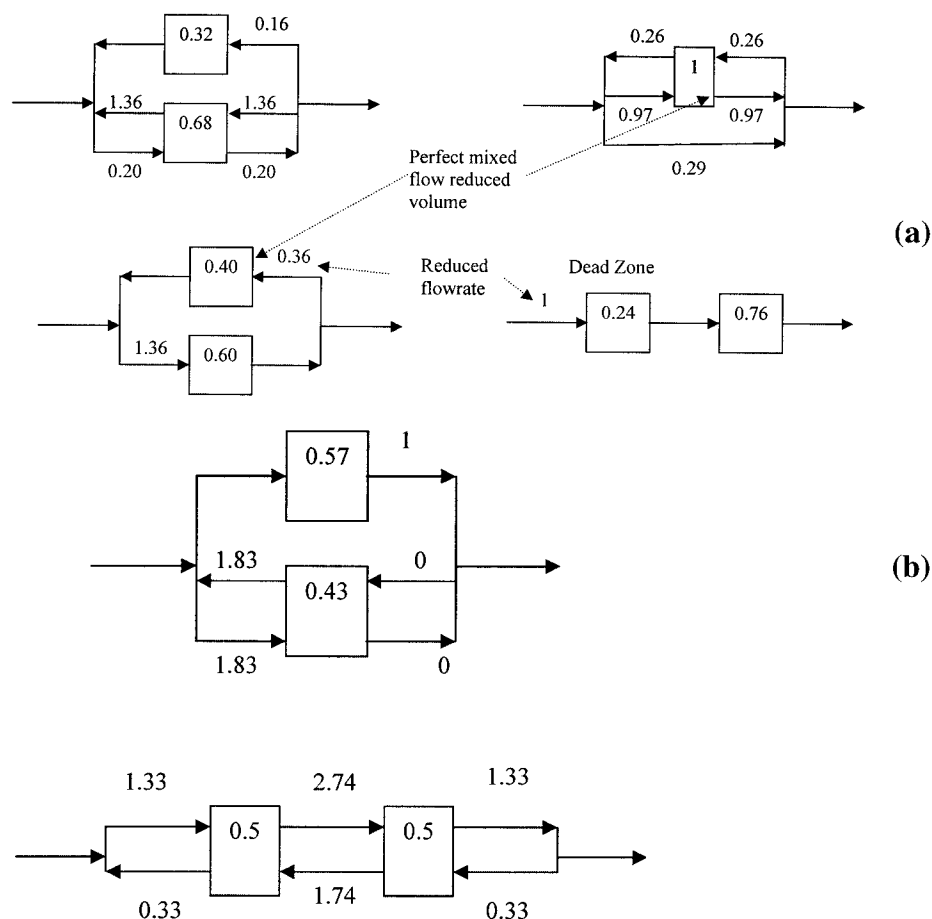


Figure 11. (a) Good solutions for case 1 ( $\lambda = 1$ ); (b) good solutions for case 2 ( $\lambda = 0$ ).

**Table 3. Design of Experiments**

Experiment	X1	X2	X3	X1X2	X1X3	X2X3	X1X2X3	I
1	–	–	–	+	+	+	–	+
2	+	–	–	–	–	+	+	+
3	–	+	–	–	+	–	+	+
4	+	+	–	+	–	–	–	+
5	–	–	+	+	–	–	+	+
6	+	–	+	–	+	–	–	+
7	–	+	+	–	–	+	–	+
8	+	+	+	+	+	+	+	+

The problem involves 29 constraints and 45 variables. The parameter  $\lambda$  is related to the studied case:

Case 1.  $\lambda = 1$  high input flow rate

Case 2.  $\lambda = 0$  low input flow rate

Case 3.  $0 < \lambda < 1$ . Find a unique structure for both cases.

### Solution strategy

Insofar as the problem involves linear and bilinear constraints, it can be solved by means of an SQP package. The major drawback of such a procedure lies in the initialization of variables. Another strategy was therefore implemented in this study, where the variables are divided into two sets: the volumes and flow rates constitute the first set and the second set involves the concentrations. Once volumes and flow rates are known, the concentrations can be computed by solving a linear system. Because the remaining constraints are all linear, a QP procedure can be used instead of an SQP one. The solution strategy is represented in Figure 10.

Because the total number of possible solutions is only of 32,768, and the CPU times are very short, an exhaustive enumeration of all the solutions is possible for the first two cases ( $\lambda = 1$  or  $\lambda = 0$ ); the CPU times (in seconds) for enumerating all the possible solutions have an order of magnitude of 10,800 and 32,000 s for  $\lambda = 1$  and  $\lambda = 0$ , respectively. The best solutions can be deduced from this enumeration and will be used in the following to fine-tune the parameters (stop criterion, length of cooling, reducing factor for the temperature) of the implemented simulating annealing procedure. The CPU time for case 3 ( $0 < \lambda < 1$ ) is more much important, given that the number of equations and constraints was practically multiplied by a factor 2 to embed both cases.

### Solution for cases 1 and 2

Recall that the function to be minimized is

$$F = (C_{f\text{mod}} - C_{f\text{exp}})^2 + \rho \sum_i y(i)^2 \quad (17)$$

**Table 4. Results of the Design of Experiments: Case 1 ( $\lambda = 1$ )**

Experiment	Success (%)	Failure (%)	CPU Time (s)
1	0	85	10.62
2	0	100	28.4
3	30	15	100.5
4	60	0	421.9
5	5	90	10.2
6	0	100	28.4
7	35	20	367.8
8	40	0	1211.3

The term  $\rho \sum_i y(i)^2$  represents the quadratic sum of elementary units involved in the current structure. The penalty coefficient value has been adjusted, so that both terms  $(C_{f\text{mod}} - C_{f\text{exp}})^2$  and  $\rho \sum_i y(i)^2$  have the same order of magnitude. Because the precision on concentrations has an order of magnitude of  $10^{-3}$ , a value of  $10^{-6}$  was chosen for the penalty coefficient. A good solution is assumed to be obtained when the quadratic deviation between the predicted and experimental concentrations (first part of the objective function  $F$ ) is less than  $10^{-20}$ . For both cases, several solutions can be identified, as reported in Figure 11a and 11b. The significant structural differences between the solutions found in both cases show the difficulty of solving the problem when the two flow rates are simultaneously considered.

### Master Problem Solution via Simulated Annealing

#### Simulated annealing procedure

At the upper level of the procedure, a simulated annealing (SA) algorithm is now implemented for extracting particular fluidized bed structures from the superstructure, by modifying the values of some integer variables.

The simulated annealing procedure mimics the physical annealing of solids, that is, the slow cooling of a molten substance, which redistributes the arrangement of the crystals (Kirkpatrick et al., 1983). In a rapid cooling or quenching, the final result would be a metastable structure with higher internal energy. The rearrangements of crystals follow probabilistic rules. In the annealing of solids, the goal is to reach given atomic configurations that minimize internal energy. In SA, the aim is to generate feasible and “good” solutions of an optimization problem with a given objective function. Because careful annealing leads to the lowest internal energy state, the SA procedure can lead to the global minimum. Given that a rapid cooling generates a higher energy metastable state, the SA procedure may avoid being trapped on a local minimum. How-

**Table 5. Values of the Effects: Case 1 ( $\lambda = 1$ )**

Effect of	On Success	On Failure
I	25	51.25
X1	2.5	1.25
X2	23.75	–42.5
X3	7.5	–0.25
X1X2	1.25	0
X1X3	0	–1.25
X2X3	8.75	–7.5
X1X2X3	1.25	0
Standard deviation	8.65	5.35
Interval size $\beta$ (at 95%)	19.5	12.15



**Table 6. Results of the Design of Experiments: Case 2 ( $\lambda = 0$ )**

Experiment	Success (%)	Failure (%)	CPU Time (s)
1	10	90	38.9
2	0	100	105.1
3	20	50	490.0
4	50	0	1876.7
5	0	100	36.5
6	0	100	107.2
7	0	50	1646.6
8	30	10	6065.4

ever, unlike classical deterministic optimization methods, a formal proof of the convergence of an SA algorithm toward a minimum does not exist.

Each structure  $S$  generated by the SA is coded on bits (15 bits for the previous example). For generating a neighboring solution  $S'$  of a given solution  $S$ , a portion of  $S$  randomly chosen, is replaced by its binary complement.

The SA parameters to be fixed are the length of the cooling stage ( $N_{sa}$ ), the initial structure, the stop criterion, the initial temperature, and the reducing factor ( $\alpha$ ) for the temperature. In the SA implemented here, the geometric scheme  $T_{i+1} = \alpha T_i$  of Kirkpatrick et al. (1982) is used. The probability of acceptance of the current solution is computed from the method proposed by Metropolis et al. (1953). The SA is stopped if the best solution is not changed during a given number of consecutive cooling stages. Like many stochastic procedures, it is recommended that the SA be executed several times on the same problem, with different initial solutions randomly generated, to reach very good solutions. A previous study (Athier et al., 1997) has shown that a good value for the initial temperature must have an order of magnitude of a fraction (1/2, 1/3) of the objective function value for the initial solution; thus, in the following examples, the initial temperature is fixed at a third of the initial objective function value.

The values of the other parameters (number of consecutive cooling stages for the stop criterion, reducing factor of the temperature, length of cooling stage) are investigated in the following section with a design of experiment procedure.

### Parametric study

The design of experiments in  $\mathbb{R}^3$  is based on an Hadamard's matrix, as shown in Table 3, where  $X1 \in [1, 5]$  represents the number of cooling stages for the stopping criterion;  $X2 \in [0.7, 0.95]$ , the reducing factor for the temperature; and  $X3 \in [2, 6]$ , the length of cooling stage expressed in terms of length of

**Table 7. Values of the Effects: Case 2 ( $\lambda = 0$ )**

Effect of	On Success	On Failure
I	13.75	62.5
X1	-6.25	2.5
X2	11.25	-35.0
X3	6.25	-10.0
X1X2	-3.75	0
X1X3	1.25	0
X2X3	8.75	-12.5
X1X2X3	-1.25	2.5
Standard deviation	8.90	5.5
Interval size $\beta$ (at 95%)	24.8	15.2

**Table 8. Influence of the Kinetic Constant: Case 1 ( $\lambda = 1$ )**

Kinetic Constant Value	Number of Units in the Solution	Number of Solutions with the Same Objective Function Value
3.5	2	22
4	2	32
4.5	2	64
5	2	64
5.5	2	64
6	2	64

structure coding ( $X3 = 2$  means that the length of the cooling stage is  $2 \times$  length of structure coding, that is, 30 for the previous example). For each experiment reported in Table 3, the SA was run 20 times with random initializations.

Two responses are studied through this design of experiments: the success rate and the failure rate. A success is assumed to occur when one of the good solutions given in Figure 11a (or Figure 11b) is obtained by the SA; a failure corresponds to a solution found by the SA, which involves at least two supplementary units than a good one.

For analyzing the design of experiments, the significance effects based on the estimation of the confidence interval are computed. It is classically assumed that the standard deviation remains constant on each experiment and, consequently, the estimation is carried out only on the median point, that is, for  $X1 = 3$ ,  $X2 = 0.825$ , and  $X3 = 4$ . As for other experiments, the SA was run 20 times on the median point. The confidence interval is of the form  $[v - \beta, v + \beta]$ , where  $v$  is the value of the concerned parameter and  $\beta$  is the size interval computed vs. the number of SA runs on each experiment from the Student's law. Recall that a parameter has a significant effect if the associated confidence interval does contain the value 0.

For case 1, the results of the design of experiments are given in Table 4 and the parameter effects are reported in Table 5, where it can be noted that only  $X2$  has a positive significant effect on the success (respectively, negative significant effect on the failure). However, the numerical efficiency of a set of parameters on the SA convergence can obviously be observed through the success and failure rates, but also through the CPU time. In this framework, a positive effect for  $X2$  corresponds to experiments 3, 4, 7, and 8, but for experiments 3 and 7 the failure rate is quite important and for experiment 8, the CPU time is high compared to that of experiment 4. Thus, in terms of global numerical efficiency, experiment 4 (that is,  $X1 = 5$ ,  $X2 = 0.95$ , and  $X3 = 2$ ) is the best one.

The same study was carried out for the low input flow rate (case 2) and the results are reported in Tables 6 and 7. The conclusion is the same as in the previous case, in which the best parameter set is always  $X1 = 5$ ,  $X2 = 0.95$ , and  $X3 = 2$ .

**Table 9. Influence of the Kinetic Constant: Case 2 ( $\lambda = 0$ )**

Kinetic Constant Value	Number of Units in the Solution	Number of Solutions with the Same Objective Function Value
4.5	2	16
5	2	15
5.5	2	16
6	2	16

**Table 10. Results for Case 3 ( $\lambda = 0.5$ )**

Number of SA	Quadratic Deviation	Number of Elements	CPU Time (s)
1	$7.7 \times 10^{-4}$	9	6707
2	$7.7 \times 10^{-4}$	9	4119
3	$7.7 \times 10^{-4}$	8	4220
4	$7.7 \times 10^{-4}$	9	3646
5	$7.7 \times 10^{-4}$	9	4508
6	$7.7 \times 10^{-4}$	9	7744
7	$7.7 \times 10^{-4}$	10	4515
8	$7.7 \times 10^{-4}$	8	5905
9	$7.7 \times 10^{-4}$	8	4592
10	$7.7 \times 10^{-4}$	8	3855

***Influence of the kinetic constant  $K$  (cases 1 and 2)***

In the previous studies, the kinetic constant  $K$  was arbitrarily fixed at 5. Its influence is now studied on cases 1 and 2. The SA was implemented with the optimal values of parameters  $X1$ ,  $X2$ , and  $X3$ . The results of this study, reported in Tables 8 and 9, show that the kinetic constant value does not affect the problem solution.

***Study of case 3 ( $\lambda = 0.5$ ): find a unique structure for high and low input flow rates***

Because the value 5 was assigned to the kinetic constant and the SA parameters were fixed at their optimal values ( $X1 = 5$ ,

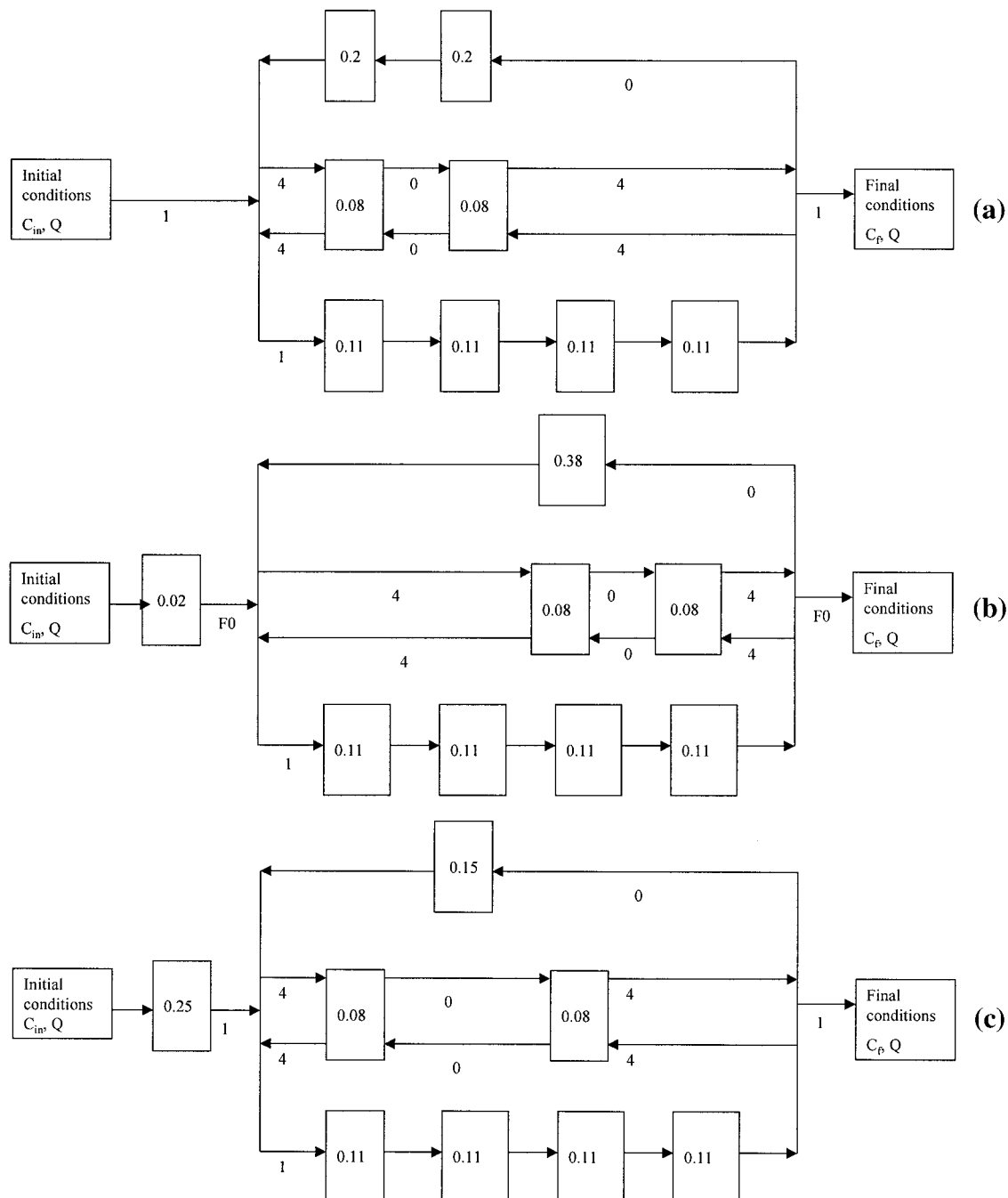


**Figure 12. (a) Best solution for the two flow rates (number of SA = 8); (b) best solution for the two flow rates (number of SA = 9); (c) best solution for the two flow rates (number of SA = 10).**

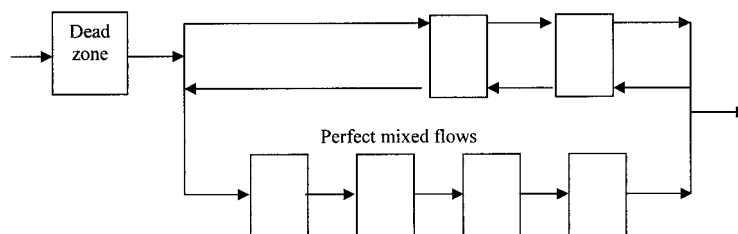


Figure 13. Solution deduced from the three solutions shown on Figure 12a–c.

$X_2 = 0.95$ , and  $X_3 = 2$ ), the case 3 study was carried out with 10 SA runs, results of which are shown in Table 10.

The quadratic deviation between the predicted and experimental concentrations (first part of the objective function  $F$ ) is always  $7.7 \times 10^{-4}$ ; for the high (respectively, low) input flow rate, the computed reactor efficiency is 0.550 (0.714), whereas the experimental value is 0.523 (0.742). The three best solutions, involving only eight elements, are shown in Figure 12a, 12b, and 12c, respectively. However, the numerical results are clearly worse than those obtained when both flow rates are considered separately.

When taking into account the flow rate values of the streams of the three solutions involving eight elements, these solutions can be simplified into a unique structure with only seven elements, as shown in Figure 13. For fluidized-bed modeling, this new structure is then optimized by using the QP procedure to determine the various volumes and flow rates.

The results obtained (see Figure 14) for the flow rates and volumes are nearly the same as those obtained for the three above solutions. Furthermore, because the flow rates between the two reactors located on the upper part of the process are null, the fluidized bed can be represented by a series of well-stirred tank reactors, where the most important part (90%) of the reaction occurs. The concentrations related to cases 1 and 2 are also reported in Figure 14. The model involves a dead zone corresponding to 40% of the total volume, so the height of the bed can be decreased without loss of efficiency. For case 1 or case 2, the error between the predicted and experimental output concentrations has an order of magnitude of 5%, so this model can be used for predicting the pellet reactor efficiency within the flow rate range considered.

ming (QP) method is developed and a pellet reactor model for phosphorus recovery from wastewater is identified as a reactor network of stirred tanks or plug flow reactors.

For solving the induced mixed integer quadratic programming (MIQP) problem, an SA generates and tests at upper-level reactor network structures, represented by binary variables related to the presence or absence of various elementary units. For each structure proposed by the SA, a QP is carried out at a lower level; the objective function to be minimized is the quadratic deviation between experimental and computed agglomeration rates, augmented with an outer quadratic function representing the number of elementary units. The goal is to find simultaneously the most appropriate model with respect to the experimental output, but also the simplest model in terms of the smallest possible number of elementary units.

For high and low input flow rates, as well as for flow rates bounded by these extreme values, the results obtained show that satisfactory reactor networks can be constructed that give good comparisons to the experimental efficiency. A major asset of this systemic approach is that the reactor efficiency can be easily deduced, without any precise knowledge of some key parameters such as the density and thickness of the calcium phosphate layer. This methodology can, of course, serve to determine the new agglomeration fluidization conditions.

Finally, from a more theoretical perspective, a methodology able to treat large-size problems for model identification was proposed and, for this purpose, simulated annealing was confirmed to be performing for the treatment of combinatorial problems, even if the optimality of the obtained solution is not demonstrated mathematically.

## Conclusions

In this article, a hybrid optimization technique that combines a simulated annealing (SA) procedure and a quadratic program-

## Notation

ACP = amorphous calcium phosphate  
 $C$  = concentration,  $\text{mg}/\text{m}^3$  or  $\text{mol}/\text{m}^3$   
 DCPD = dicalcium phosphate dihydrate

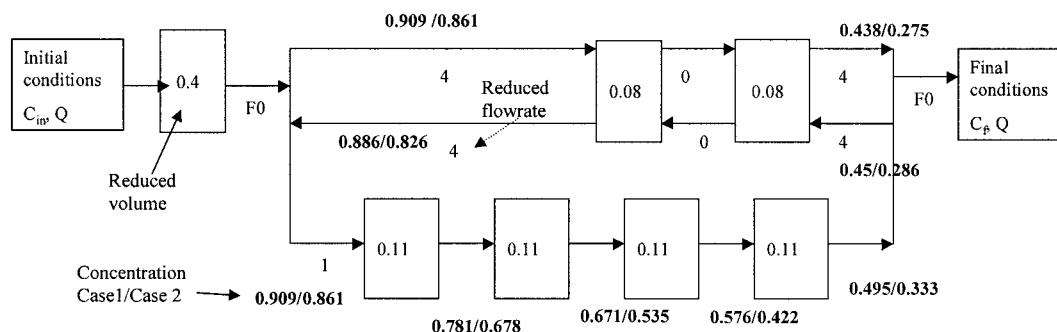


Figure 14. Solution proposed for the two flow rates.

$F$  = flow rate, m<sup>3</sup>/h  
 $K$  = kinetic constant, m<sup>3</sup> s<sup>-1</sup>  
 MINLP = mixed integer nonlinear programming  
 MIQP = mixed integer quadratic programming  
 $N$  = particle concentration, m<sup>-3</sup>  
 $Nsa$  = length of the cooling stage  
 $P$  = phosphate  
 $Q$  = flow rate, L/h  
 QP = quadratic programming  
 SA = simulated annealing  
 SQP = successive quadratic programming  
 $T$  = temperature, °C  
 $t$  = time, s  
 $V$  = volume, L or m<sup>3</sup>  
 $X$  = conversion of phosphate from liquid to solid phase  
 $y$  = vector of integer variables  $y_i$

### Greek letters

$\alpha$  = reducing temperature factor  
 $\varepsilon$  = bed porosity  
 $\eta$  = phosphate removal efficiency  
 $\eta_{agg}$  = agglomeration rate  
 $\rho$  = penalty coefficient

### Subscripts

$i$  = fines  
 $j$  = grains

### Literature Cited

- Athier, G., P. Floquet, L. Pibouleau, and S. Domenech, "Synthesis of Optimum Heat Exchanger Networks by Simulated Annealing," *AIChE J.*, **43**(11), 3007 (1997).
- Floquet, P., L. Pibouleau, and S. Domenech, "Identification de modèles par une méthode d'optimisation en variables mixtes," *Entropie*, **151**, 28 (1989).
- Hirasawa, I., and Y. Toya, "Fluidized-Bed Process for Phosphate Removal by Calcium Phosphate Crystallization," *ACS Symp. Ser.*, **438**, 355 (1990).
- Kirkpatrick, S., C. D. Gelatt, and M. P. Vecchi, "Simulated Annealing: Theory and Applications," *IBM Res. Rep.*, RC 9355 (1982).
- Kirkpatrick, S., C. D. Gelatt, and M. P. Vecchi, "Optimization by Simulated Annealing," *Science*, **220**, 671 (1983).
- Laquerbe, C., J. C. Laborde, S. Soares, P. Floquet, L. Pibouleau, and S. Domenech, "Synthesis of RTD Models via Stochastic Procedures: Simulated Annealing and Genetic Algorithm," *Comput. Chem. Eng.*, **25**, 1169 (2001).
- Metropolis, N., A. Rosenbluth, M. Rosenbluth, A. Teller, and E. Teller, "Equation of State Calculations by Fast Computing Machines," *J. Chem. Phys.*, **21**, 1087 (1953).
- Montastruc, L., C. Azzaro Pantel, B. Biscans, M. Cabassud, and S. Domenech, "A Thermochemical Approach for Calcium Phosphate Precipitation Modeling in a Pellet Reactor," *Chem. Eng. J.*, **94**(1), 41 (2003).
- Montastruc, L., C. Azzaro Pantel, M. Cabassud, and B. Biscans, "Calcium Phosphate Precipitation in a Pellet Reactor," Proc. of 15th Int. Symp. on Industrial Crystallization: Design and Operation of Crystallizers, Sep. 15–18 2002, Sorrento, Italy, Vol. 3, pp. 1251–1256 (2002).
- Morse, G. K., S. W. Brett, J. A. Guy, and J. N. Lester, "Review: Phosphorus Removal and Recovery Technologies," *Sci. Total Environ.*, **212**, 69 (1998).
- Mullin, J. W., *Crystallization*, 3rd ed., Butterworth Heinemann, London (1993).
- Seckler, M. M., O. S. L. Bruinsma, and G. M. van Rosmalen, "Phosphate Removal in a Fluidized Bed—2. Process Optimization," *Water Res.*, **30**(7), 1589 (1996).

Manuscript received Jun. 17, 2003, and revision received Jan. 29, 2004.